MedCrave
Step into the World of Research
Journal of Analytical & Pharmaceutical research

Research Article

Open Access
CrossMark

Inhibition of zinc corrosion by glycerol stearate in 1.0M hydrochloric acid medium with experimental, theoretical, and electrochemical techniques

Abstract

Glycerol Stearate (GS) was investigated as a corrosion inhibitor via weight loss on zinc (Zn) metal inside 1.0M hydrochloric acids (HCl). Different electrochemical techniques such as potentiodynamic polarization (PDP), electrochemical impedance spectroscopy (EIS) and characterization methods were used in the study. Weight loss measurements and inhibition efficiency (IE) were used to calculate the amount of weight loss and to scrutinize the effect of inhibition concentration on the metal in HCl, and it demonstrated that weight loss decreased as the inhibition concentration increased, and percentage inhibition efficiency increased with increasing inhibition concentration. The Corrosion rate (ρ) was calculated, and it was observed that it decreased with the increasing inhibition concentration but increased with an increase in temperature. The compound of inhibitor effectively prevented corrosion by becoming adsorbed to the metal surface and was confirmed by Fourier transform infrared spectroscopy (FTIR). Free Gibbs energy (FGE) demonstrated a spontaneous corrosion process at the metal surface of zinc and the scanning electron microscope (SEM) was used to investigate the surface morphology of the protective layer and confirmed that the adsorption of glycerol stearate was via physisorption adsorption. The adsorption of glycerol stearate on the metal surface was found to follow the Langmuir adsorption isotherm model.

Keywords: zinc metal, glycerol stearate, corrosion inhibition, weight loss, corrosion rate, adsorption, inhibitor concentration, inhibition efficiency

Volume 12 Issue 2 - 2023

Thabo Pesha,[1] Vusimuzi L Mulaudzi,[1] Peace P Mkhonto,[2] Mmaphefo P Mothapo,[1] Terrence Mothlathlo[1]

[1]Department of Chemistry, School of Physical and Mineral Sciences, Faculty of Science and Agriculture, University of Limpopo (Turfloop Campus), Private Bag X1106, Sovenga 0727, South Africa

[2]Department of Physics, Materials Modelling Centre, School of Physical and Mineral Sciences, Faculty of Science and Agriculture, University of Limpopo (Turfloop Campus), Private Bag X1106, Sovenga 0727, South Africa

Correspondence: Vusimuzi Ludwig Mulaudzi, School of Physical and Mineral Sciences, Faculty of Science and Agriculture, University of Limpopo (Turfloop Campus), Polokwane, Private Bag X1106, Sovenga 0727, South Africa, Tel 0152683240, Email vusimuzi.mulaudzi@ul.ac.za

Received: April 15, 2023 | **Published:** May 02, 2023

Introduction

Corrosion is the natural process that occurs when native metals are transformed into undesirable substances when they react with substances like water or air.[1] This process undergoes a redox reaction whereby metals act as the reducing agent, losing electrons, and the oxygen (in water and air) act as the oxidizing agent, receiving electrons, causing the reaction to be spontaneous and electrochemically favoured. The damage to the metals caused by this reaction begins from the tiny part of the metal exposed to a corrosive environment which then leads to rusting.[2] When the metal is subjected to the rusting, hydroxyl ions (OH) occur when the electrons on the oxygen, and the hydrous iron oxide $Fe(OH)_3$ is formed through the reaction of hydroxyl ions and Fe^{3+}: $Fe^{3+} + 3OH^- \rightarrow Fe(OH)_3$ (Overall equation).

Corrosion has been identified as a major problem in olefin applications due to the loss of materials such as pipes, especially in oilfields. Oil and gas-producing industries are negatively affected by corrosion worldwide every year, which results in a great loss of costs and a negative impact on the economy.[3] The economic loss of corrosion worldwide is estimated to be greater than $2.5 trillion, while in South Africa it is R130 billion.[4] This was conducted by the University of Witwatersrand and the Corrosion Institute of Southern Africa. Most companies transport the products through pipelines and tanks, which get into contact with water and interact with air. After the reaction of oxygen and water, the rust is generated which then flows with the compressed air inside the steel pipes, attacking them from the small portion to the entire metal. The use of inhibitors has been identified as the method for preventing corrosion.

Corrosion inhibitors are substances that prevent or decrease the rate of corrosion on metals.[5] This is done by coating, plating, cathodic protection, and anodic protection of the surface of the metal or by immersing the metal inside the inhibitor solution. In addition, sodium hydroxide (NaOH) and sodium carbonate (Na_2CO_3) are the most used inhibitors; since they increase pH near metals which reduces the transportation of oxygen to the metal surface. Other organic compounds such as heterocyclic compounds are effective and form a hydrophobic film on the metal surface. In this study, the use of the glycerol stearate in Figure 1 is reckoned as a part of the green chemistry inhibition method. The concentrations of the inhibitor decrease the rate of corrosion, especially the higher concentrations than the lower ones. The prevention occurs by immersing the metal inside the inhibition solution.[6] The metal absorbs the inhibitor on its surface, forming a protective film and preventing oxygen or water to attack. Furthermore, temperature has been identified as one of the factors affecting the rate of corrosion.

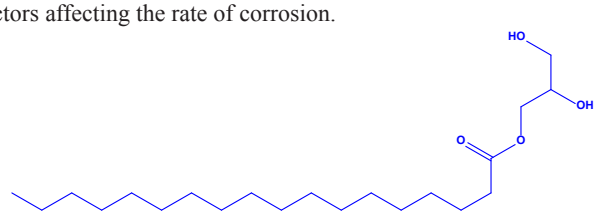

Figure 1 Molecular structure of glycerol stearate.

Materials and methods

Glycerol stearate was purchased from Prestige laboratory supplies, South Africa. Zinc metal sheets were prepared and purchased from the University of Northwest, South Africa, and 32% Hydrochloric acid (HCl) was purchased at Rochelle Chemicals, South Africa.

Gravimetric method

Three zinc metals with the specimen of 3 cm x 4 cm were weighed and immersed inside 100 ml beakers containing a blank solution of

1.0 M prepared from 32% Hydrochloric acid. The metals were again completely immersed inside 100 ml beakers containing different glycerol stearate concentrations, 10 x 10^{-5} M, 30 x10^{-5} M and 50 x 10^{-5} M inside 1.0 M Hydrochloric acid and placed inside three thermostats at temperatures of 318 K, 328 K and 338 K, constituting three sets of experiments. After the time has elapsed, the metals were removed from the thermostats and washed with distilled water, then rinsed with acetone. They were dried for 5 to 10 minutes then re-weighed, and the final masses were recorded. The experimental time for metal immersion in the absence and presence of an inhibitor was 3 hours.

The corrosion rate (ρ in g.cm^{-2}.h^{-1}), percentage inhibition efficiency (%I), and surface coverage (θ) were calculated from the weight loss using the equations below.[7]

$$\rho = \frac{\Delta W}{St} \quad (1)$$

$$\theta = \left(\frac{\rho_1 - \rho_2}{\rho_1} \right) \quad (2)$$

$$\%\,\mathrm{I} = \left(\frac{\rho_1 - \rho_2}{\rho_1} \right) X 100 \quad (3)$$

Where ΔW denoted zinc average weight loss, S denoted total surface area of the zinc specimen (cm^2), *and* t denoted immersion time (h), while ρ_1 and ρ_2 were corrosion rates with and without inhibitors respectively.

Characterization technique

The inhibitor was confirmed by the Spectrum II FTIR spectrometer (PerkinElmer). The spectrum was within 500 and 4000 cm^{-1} at a resolution of 4 cm^{-1}. Scanning electron microscopy (SEM) was used to perform morphological analysis on the samples. SEM was used on a TESCAN Vega TC using TESCAN software, together with energy dispersive X-ray spectroscopy (EDXS) to determine the elemental composition of the samples (at 20 kV). The samples were gold-coated to enhance imaging by forming a conductive layer on the analytes' surfaces, which prevented charging and elemental composition interference.

Adsorption studies

During the corrosion testing in the presence of the inhibitor compound, an adsorptive film was formed on a zinc surface, and an oxide layer was further characterized using the FTIR technique, which was essential in studying the protective layer formed on the metal surface. This technique allowed for the analysis of both liquid and solid samples. In the FTIR technique, the infrared absorption spectrum was measured, and another advantage was that the technique is fast in processing data. Furthermore, the functional groups of the chemical inhibitor molecule were investigated using FTIR qualitative analysis.

Electrochemical measurement

Electrochemical parameters were obtained with the aid of the Bio-Logic SP150 potentiostat working station, which consisted of a three-electrode cell, namely, saturated calomel electrode (SCE), reference electrode (RE), platinum counter electrode (CE) and Zn metal (1cm^2) working electrode (WE) without and with corrosion inhibitor concentrations. Potentiodynamic polarization studies were conducted between -0.250 and +0.250 mV scanning range at a 1.0 mV/s constant sweep rate on the open circuit potential (OCP). Both anodic and cathodic polarization graphs were achieved when stabilization was attained after the working electrode was immersed for 30 min in the test solution. Electrochemical impedance (EIS) measurements were conducted by employing a 100 kHz to 10 Hz frequency range with a 10 mV peak-to-peak voltage, using an alternating current (AC) signal at corrosion potential.

Potentiodynamic polarization

To obtain the relevant electrochemical parameters such as the E_{corr}, i_{corr} anodic Tafel slope, b_a and cathodic Tafel slope, b_c, the potentiodynamic polarization method was used. According to Equation 4, the current densities measured were used to calculate the percentage inhibition efficiency of the chemical corrosion inhibitor compound.[8]

$$\%\,\mathrm{I_{PDP}} = \left(1 - \frac{i^{i}_{corr}}{i^{0}_{corr}} \right) x 100 \quad (4)$$

corrosion current density values were denoted by i^{0}_{corr} and i^{i}_{corr} denoting the corrosion current density in the absence and in the presence of an inhibitor respectively.

Electrochemical impedance spectroscopy

Electrochemical impedance spectroscopy was utilized for studying charge transfer resistance occurring during the corrosion of zinc metal in a corrosive environment. This technique was used to evaluate electrochemical measurements including solution resistance (R_s), charge transfer resistance (R_{ct}) with the inhibitor and charge transfer resistance (R^{o}_{ct}) without the inhibitor, double layer capacitance (d_{11}), the constant phase element (CPE), and exponents, which were further investigated by employing EIS. Furthermore, Equation 5, R_{ct} and R^{o}_{ct} were used to calculate the inhibition efficiency:[8]

$$\%\,\mathrm{I}_{EIS} = \left(1 - \frac{R^{o}_{ct}}{R_{ct}} \right) x 100 \quad (5)$$

Results and discussion

Weight loss measurements

Effect of inhibitor concentration and temperature on corrosion rate

The gravimetric experiments of glycerol stearate (GS) inhibitor were presented by the percentage inhibition efficiencies (%IE) against inhibitor concentration plots at 318, 328 and 338 K as given in Figure 2A. The %IE was observed to increase as the inhibitor concentration increased from 10 x 10^{-5} - 50 x 10^{-5} M, for GS. In addition, it was observed that the %IE decreased with the increase in temperature. The effect of temperature was shown by the %IE values for 10 x 10^{-5} M at 318 K, 67.16% while at 328 and 338 K, 68.65% and 73.13% were obtained respectively. The density of the corrosion rate increased severely as the temperature increased. As shown from studies, the rate of metal dissolution was hindered by increasing the inhibitor concentration. The corrosion rate was found to be 15.56, 19.44 and 31.11 × 10^{-3} g.cm^{-2}.h^{-1} in the uninhibited solution at 318, 328 and 338 K, respectively. However, according to the observations in Table 1 it was observed that upon the introduction of the inhibitor in the solution, the rate of corrosion decreased. A similar behaviour was observed by Hong et al.[9] using fungicides and 4-amino-antipyrine on the corrosion of copper in NaCl solution, respectively. It was found that the metal dissolution decreased optimum to a value of 10.0× 10^{-3}g. cm^{-2}. h^{-1} in GS for 50 x 10^{-5} M inhibitor concentration at 318 K. Furthermore, metal weight loss decreased with a decrease in the rate of corrosion due to the inhibitor adsorption on Zn metal surface.

The mechanism type followed during the process of adsorption at the inhibitor/metal interface has been investigated in a significant

way by fitting various adsorption isotherms with the best regression line R^2 value. Figure 2B depicted a Langmuir adsorption isotherm plot with R^2 values ranging from 0, 9996 to 0, 9999. The Langmuir plots were enhanced by R^2 values close to unity. Table 2 showed the adsorption equilibrium constant and standard free energy of adsorption values. The number of inhibitor layers that had been adsorbed on the metal surface was calculated by using the slopes of the regression lines. The standard free energy of adsorption.[10] offered insight into the spontaneity of the inhibitory process as well as the stability of adsorption. According to the research that has been done.[11] A spontaneous process was characterized by having values of free energy of adsorption that are on the negative sign. In addition, a physisorption adsorption mechanism is indicated when the value of the free energy of adsorption is less than or equal to -20 kJ. mol^{-1}, whereas a chemisorption adsorption mechanism is indicated when the value is greater than or equal to -40 kJ. mol^{-1} in the negative direction.[12] GS supplied a physisorption process, which can be found displayed in Table 2, for Gibbs free energy values that were lower than -20 kJ. mol^{-1}.

Thermodynamic and activation parameters

Metal dissolution increased with the increase in temperature, and as a result, there was a lower activation barrier.[13] With the help of the Arrhenius equation and plot, the effect of temperature on the adsorption of GS onto the Zn surface was evaluated. The log ρ against the 1/T plot was shown in Figure 2C. The plot assisted in calculating the values of the activation energy for the corrosion process. Table 3 showed records of the calculated parameters of activation energy with the aid of Equation 6. The activation energy value in the uninhibited solution was less than those obtained in the inhibited solution. Higher activation energy values in the inhibited solution advocated a prolonged rate of corrosion due to the formation of the GS/Zn complex.[14] The entropy and enthalpy of activation can be used to investigate the inhibition efficiency of GS on the Zn metal surface. Scientists have found that higher negative entropy values represented less surface destruction on metal, while higher positive entropy values represented greater disorder in the system.[15]

$$\log \rho = \log A - \frac{Ea}{2.303RT} \quad (6)$$

Enthalpy values can represent either endothermic or exothermic reactions, depending on the sign of the value. Adsorption can be either physically or chemically involved in exothermic processes.[16,17] The plot of the transition was shown in Figure 2 (D) with the aid of Equation 7:

$$\log\left(\frac{CR}{T}\right) = \left[\log\left(\frac{R}{hN}\right) + \left(\frac{\Delta S}{2.303R}\right)\right] - \frac{\Delta H}{2.303RT} \quad (7)$$

Potentiodynamic polarization (PDP)

The polarization parameters can be determined with the help of tafel plots. These include the corrosion potential (E_{corr}), the corrosion current density (I_{corr}), the anodic tafel slope (b_a), and the cathodic tafel slope (b_c). Corrosion current densities were calculated by extrapolating tafel segments from anodic and cathodic curves. Coefficients of inhibition were found to be proportional to densities of corrosion currents (Equation 4).[18] In Figure 3 shown was the tafel plot for zinc metal in 1.0M HCl at varying concentrations of the GS inhibitor compound, both in its uninhibited form and its inhibited form. The addition of glycerol stearate corrosion inhibitor was found to decrease I_{corr} values. Inhibitor adsorption onto the zinc metal surface was observed, providing support for the adsorption mechanism.[18] Furthermore, the calculated E_{corr} difference between the blank (1. 0 M HCl) and the inhibitor solutions was less than 85 mV, which indicated a mixed-type mechanism of inhibition with the cathodic mechanism dominating as observed from the tafel slopes at each inhibitor concentration (Table 4).[8]

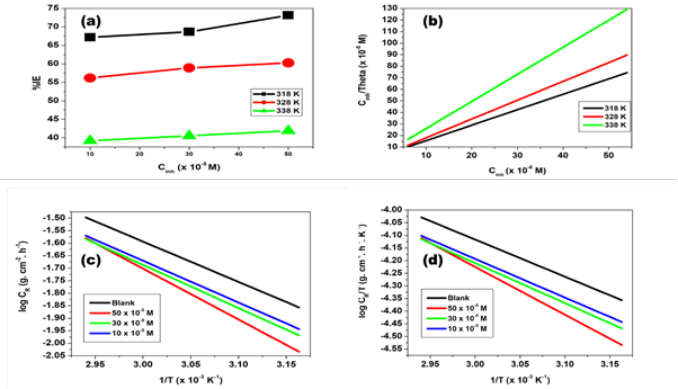

Figure 2 Efficiency (%IE) versus GS concentration (M) plot for (a) GS; and Langmuir isotherm (b) GS inhibitor on a zinc sheet at 318 K, 328 K and 338 K. Arrhenius graphs for zinc metal in 1. 0 M HCl with and without GS (c) Transition state graphs at differing GS (d).

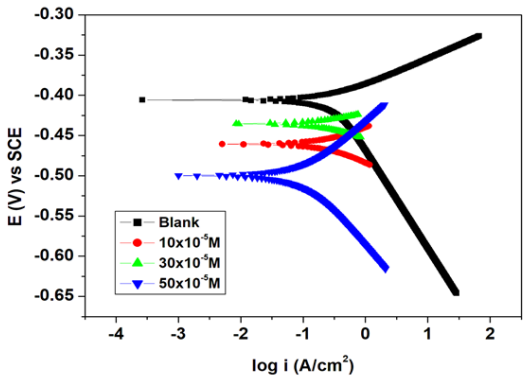

Figure 3 Potentiodynamic polarization plot for zinc in 1. 0 M HCl in the uninhibited and inhibited solutions of GS different concentrations.

Electrochemical impedance

Further study of corrosion behaviour zinc metal in acidic medium in the uninhibited and inhibited solution of GS at different concentrations was conducted. In Figure 4 & 5 shown was a representation of Nyquist plot and its corresponding bode plot for zinc metal in the absence and presence of GS inhibitor compound. Bode plots revealed some information with regards to electrochemical behaviour of both the uninhibited and inhibited systems, it was revealed that at higher phase angle there was a frequency shift to higher frequency in the presence of glycerol stearate concentrations. It was studied that the imperfection of the semicircles in the impedance spectra of zinc was due to the roughness and inhomogeneity on the metal surface.[18] From Table 5 shown was the impedance data for zinc metal obtained. Table 5 showed that the charge transfer resistance (R_{ct}) increased as the inhibitor concentration increased. The highest efficiency of 89.50% was obtained at 50 x 10^{-5} M. Moreover, to define the impedance nature, an equivalent electric circuit made up of the solution resistor (R_s), charge transfer resistance (R_{ct}) and a double layer capacitance (C_{d1}) in Figure 6 was utilized. Furthermore, Figure 5 showed bode

plots with phase angle of approximately 70 °C at the highest inhibitor concentration. Moreover, the phase angle was observed to increase as the inhibitor concentration increased and this was complimented by the frequency plot in Figure 5.

Table 1 Corrosion rate (ρ), the efficiency of inhibition, (%IE) and surface coverage (θ) of GS at 318, 328 and 338 K for zinc metal

Inhibitor	Temperature (K)	Concentration (x 10^{-5} M)	Weight loss (g)	Corrosion rate (x 10^{-3} g. cm^{-2}. hr^{-1})	Inhibition efficiency (IE)	Surface coverage (Θ)	C/Θ x 10^{-5}
GS	318	0	0.28	15.56	_	_	_
		10	0.22	12.22	67.16	0.6716	14.8893
		30	0.21	11.67	68.65	0.6865	43.6968
		50	0.18	10.0	73.13	0.7313	68.3688
	328	0	0.35	19.44	_	_	_
		10	0.32	17.78	56.17	0.5617	17.8034
		30	0.30	16.67	58.91	0.5891	50.9263
		50	0.29	16.11	60.28	0.6028	82.9486
	338	0	0.56	31.11	_	_	_
		10	0.45	25.00	39.19	0.3919	25.5183
		30	0.44	24.44	40.54	0.4054	74.0029
		50	0.43	23.89	41.89	0.4189	119.3593

Table 2 Adsorption parameters for glycerol stearate on zinc

Inhibitor	Temperature (K)	Adsorption equilibrium constant (x10^5 L.mol^{-1})	Coefficient of determination	Free Gibbs energy (kJ.mol^{-1})
GS	318	0.4528	0.9989	-8.52
	328	0.5881	0.9999	-8.79
	338	0.3877	0.9996	-9.06

Table 3 Presented are activation energy (E_a), entropy (ΔS°) and enthalpy of activation (ΔH°_a) values for zinc metal

Inhibitor	Concentration (x10^{-5}M)	Activation energy (kJ.mol^{-1})	enthalpy of activation (kJ.mol^{-1})	Entropy (JK^{-1}.mol^{-1})
GS	0	30.85	28.13	-197.30
	10	31.98	29.26	-197.20
	30	33.03	30.30	-197.05
	50	38.94	36.21	-196.14

Table 4 Polarization measurements such as E_{corr}, I_{corr}, b_a and b_c using different inhibitor concentrations

Inhibitor	Concentration x 10^{-5} (M)	$-E_{corr}$ (mV)	I_{corr} (mA.cm^{-2})	b_a (mV)	b_c (mV)	$\%IE_{PDP}$
Blank		445.25	0.38	70.3	97.5	-
GS	10	460.79	0.28	36.1	40.3	26.32
	30	435.47	0.19	18.5	25.3	50.00
	50	499.87	0.11	69.4	91.5	71.05

Table 5 Electrochemical impedance parameters

Inhibitor	Concentration x 10^{-5} (M)	Solution resistance (Ω)	Charge transfer resistance (Ω)	Double layer capacitance (x10^{-6} F)	Inhibition efficiency
Blank		2.348	6.429	0.418	-
GS	10	2.344	11.54	0.252	44.29
	30	3.109	16.94	0.419	62.05
	50	2.121	61.24	0.006	89.50

Adsorption studies

In the FTIR spectrum (Figure 7) of the adsorption film, a disappearance of the following bands was observed, such as hydrogen bonds (3307 cm^{-1} and 3241 cm^{-1}) formed by hydroxyl group, CH_2 stretch of alkyl carbon chains (2914 cm^{-1} and 2849 cm^{-1}), another visible peak occurring at 1730 cm^{-1} accredited to the C=O stretching mode. This behaviour owed to the successful interaction between glycerol stearate and the zinc metal surface.

Morphological studies

Figure 8 displayed the pristine zinc metal with about 95.1% composition as shown by the EDXS spectrum, in addition, the micrograph showed smooth surface abrasions caused by the emery papers. Figure 9 displayed a micrograph with a tempered surface due to the presence of the Cl^- (present in 6.8% composition shown on the EDXS) ion from the hydrochloric solution which facilitated the zinc metal dissolution. Finally, Figure 10 displayed SEM micrograph with

the formation of agglomerations due to the presence of the glycerol stearate with the O atom (15.8% composition) which reduced the Cl^- ion to 0.7% composition as compared to Figure 9 thus a successful inhibition of the metal dissolution.

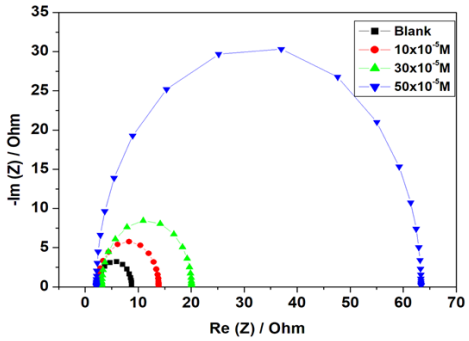

Figure 4 Nyquist plot for zinc in 1.0 M HCl in the uninhibited and inhibited solution with different GS concentrations.

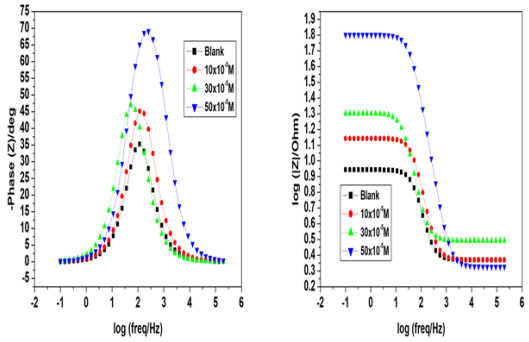

Figure 5 Bode plots of zinc in 1.0 M HCl with and without glycerol stearate.

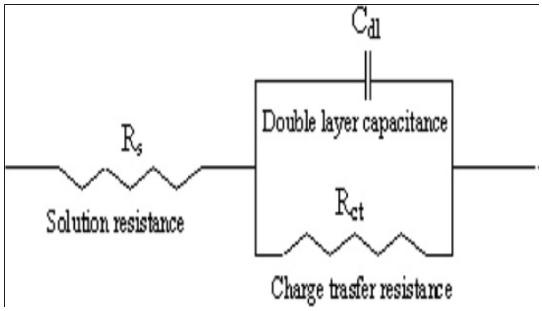

Figure 6 The proposed electrical circuit for studied glycerol stearate.

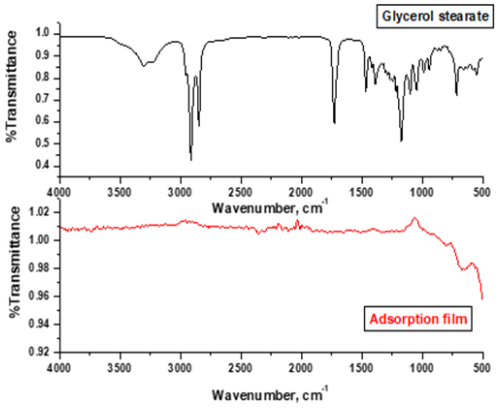

Figure 7 Adsorption film studies of glycerol stearate on zinc metal surface.

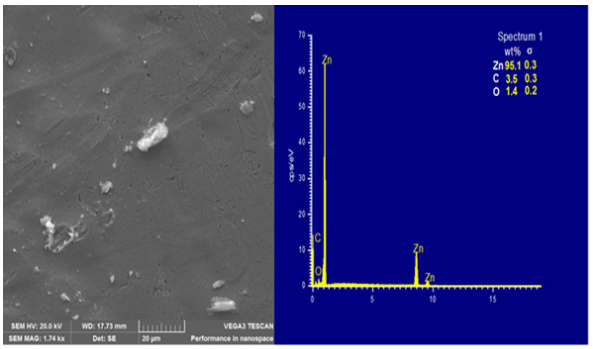

Figure 8 SEM micrograph and EDXS spectrum of pristine zinc.

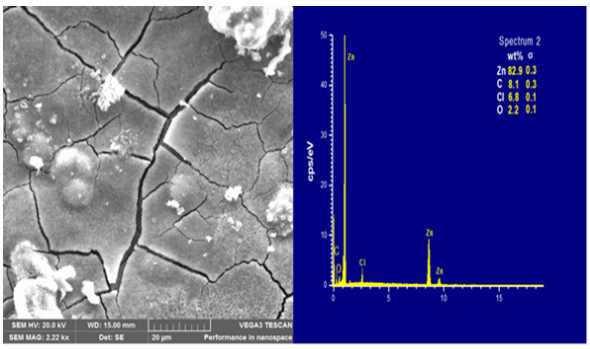

Figure 9 SEM micrograph and EDXS spectrum of zinc in 1.0 M HCl.

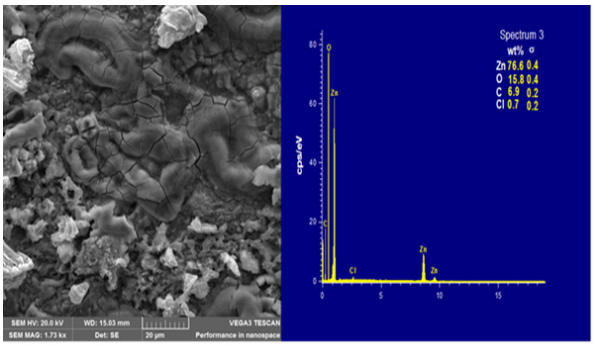

Figure 10 SEM micrograph and EDXS spectrum of zinc in 1.0 M HCl and glycerol stearate inhibition.

Conclusion

Glycerol Stearate was found to be a good corrosion inhibitor, and this was supplemented by the inhibition efficiency results (73.13%, 71.05% and 89.50%) obtained through weight loss, potentiodynamic polarization, electrochemical impedance spectroscopy at 50 x 10^{-5} M, respectively. In addition, inhibition efficiency increased with the increase in the glycerol stearate. The rate of corrosion rate (ρ), current density was observed to reduce and charge transfer resistance was observed to increase in the presence of the increasing glycerol stearate concentrations. Furthermore, from weight loss measurements, the inhibition efficiency values were observed to decrease with the increase in temperature. Glycerol stearate effectively prevented corrosion by adsorbing to the metal surface and this was confirmed by Fourier transform infrared spectroscopy. Negative values of the free Gibbs energy demonstrated a spontaneous corrosion process. The morphology of the metal surface of the pristine metal, metal in corrosive medium and metal in the presence of the inhibitor

Citation: Pesha T, Mulaudzi VL, Mkhonto PP, et al. Inhibition of zinc corrosion by glycerol stearate in 1.0M hydrochloric acid medium with experimental, theoretical, and electrochemical techniques. *J Anal Pharm Res.* 2023;12(2):60–66. DOI: 10.15406/japlr.2023.12.00424

were varied with the aid of the scanning electron microscopy. The adsorption of glycerol stearate on the metal surface was found to follow the Langmuir adsorption isotherm model.

Acknowledgments

This work was financially supported by the National Research Foundation (NRF) and the Sasol foundation. University of Limpopo, South Africa. Dr. T Pesha would also love to acknowledge Mintek, Dr. A. N. Jijana, Dr. P Mkhonto and Mr. T.G. Tsoeunyane at the University of Johannesburg (Doornfontein) for helping with electrochemical experiments.

Conflicts of interest

The authors declare that they have no known competing financial interests or personal relationships that could have appeared to influence the work reported in this paper.

References

1. Kokilaramani S, Rajasekar MM, Govarthanan M, et al. Microbial influenced corrosion of processing industry by re-circulating wastewater and its control measures-A review. *Chemosphere*. 2021;265:129075.
2. Asri RIM, Harun WSW, Samykano M, et al. Corrosion and surface modification on biocompatible metals: A review. *Materials Science and Engineering*. 2017;77:1261–1274.
3. Soltanieh M, Zohrabian A, Holyport MJ, et al. A review of global gas flaring and venting and impact on the environment: Case study of Iran. *International Journal of Greenhouse Gas Control*. 2016;49:488–509.
4. Verma C, Ebenso EE, Quraishi MA. Ionic liquids as green and sustainable corrosion inhibitors for metals and alloys: an overview. *Journal of Molecular Liquids*. 2017;233:403–414.
5. Peter A, Obot IB, Sharma SK. Use of natural gums as green corrosion inhibitors: an overview. *International Journal of Industrial Chemistry*. 2015;6(3):153–164.
6. Vigdorovich VI, Tsygankova LE, Shel NV, et al. Protection of carbon steel against atmospheric corrosion by volatile inhibitors of IFKhAN series at high concentrations of CO2, H2S and NH3. *International Journal of Corrosion and Scale Inhibition*. 2018;7(2):175–184.
7. Verma DK, Khan F. Green approach to corrosion inhibition of mild steel in hydrochloric acid medium using extract of spirogyra algae. *Green Chemistry Letters and Reviews*. 2016;*9*(1):52–60.
8. Pesha T, Mulaudzi VL, Cele ML, et al. Evaluation of corrosion inhibition effect of glycerol stearate on aluminium metal by electrochemical techniques. *Arabian Journal of Chemistry*. 2023;16(7):104798.
9. Sakthivel A, Jeyasubramanian K, Thangagiri B, et al. Recent advances in Schiff base metal complexes derived from 4-aminoantipyrine derivatives and their potential applications. *Journal of Molecular Structure*. 2020;1222:128885.
10. Guo L, Tan J, Kaya S, et al. Multidimensional insights into the corrosion inhibition of 3, 3-dithiodipropionic acid on Q235 steel in H2SO4 medium: a combined experimental and in silico investigation. *J Colloid Interface Sci*. 2020;570:116–124.
11. Murulana LC, Kabanda MM, Ebenso EE. Investigation of the adsorption characteristics of some selected sulphonamide derivatives as corrosion inhibitors at mild steel/hydrochloric acid interface: Experimental, quantum chemical and QSAR studies. *Journal of Molecular Liquids*. 2016;215:763–779.
12. Kolo AM, Idris S, Bamishaiye OM. Corrosion inhibition potential of ethanol extract of Bryophyllum pinnatum leaves for zinc in acidic medium. *Edelweiss Applied Science and Technology*. 2018;2:18–25.
13. Li T, Wu J, Guo X, et al. Activation energy of metal dissolution in local pit environments. *Corrosion Science*. 2021;193:109901.
14. Ammal PR, Prajila M, Joseph A. Effective inhibition of mild steel corrosion in hydrochloric acid using EBIMOT, a 1, 3, 4-oxadiazole derivative bearing a 2-ethylbenzimidazole moiety: electro analytical, computational, and kinetic studies. *Egyptian Journal of Petroleum*. 2018;27(4):823–833.
15. Wang W, Li F, Wang H. The effect of tetrethylenepentamine (TEPA) on the oxidation stability and the lubrication performance of biodiesel. *Industrial Crops and Products*. 2021;171:113910.
16. Leng CZ, Losego MD. A physiochemical processing kinetics model for the vapor phase infiltration of polymers: Measuring the energetics of precursor-polymer sorption, diffusion, and reaction. *Physical Chemistry Chemical Physics*. 2018;20(33):21506–21514.
17. Ammendola P, Raganati F, Chirone R. CO2 adsorption on a fine activated carbon in a sound assisted fluidized bed: Thermodynamics and kinetics. *Chemical Engineering Journal*. 2017;322:302–313.
18. Tsoeunyane MG, Makhatha ME, Arotiba OA. Corrosion inhibition of mild steel by poly (butylene succinate)-L-histidine extended with 1, 6-diisocynatohexane polymer composite in 1 M HCl. *International journal of corrosion*; 2019.